

The Neutral Hydrogen Content of Fornax Cluster Galaxies

Anja Schröder¹, Michael J. Drinkwater², and O.-G. Richter³

¹ Observatoire de la Côte d’Azur, B.P. 4229, 06304 Nice Cedex 4, France

² School of Physics, University of Melbourne, Victoria 3010, Australia

³ Hamburger Sternwarte, Gojenbergsweg 112, 20119 Hamburg, Germany

Received date; accepted date

Abstract. We present a new set of deep HI observations of member galaxies of the Fornax cluster. We detected 35 cluster galaxies in HI. The resulting sample, the most comprehensive to date, is used to investigate the distribution of neutral hydrogen in the cluster galaxies.

We compare the HI content of the detected cluster galaxies with that of field galaxies by measuring HI mass-to-light ratios and the HI deficiency parameter of Solanes et al. (1996). The mean HI mass-to-light ratio of the cluster galaxies is 0.68 ± 0.15 , significantly lower than for a sample of HI-selected field galaxies (1.15 ± 0.10), although not as low as in the Virgo cluster (0.45 ± 0.03). In addition, the HI content of two cluster galaxies (NGC 1316C and NGC 1326B) appears to have been affected by interactions. The mean HI deficiency for the cluster is 0.38 ± 0.09 (for galaxy types $T=1-6$), significantly greater than for the field sample (0.05 ± 0.03). Both these tests show that Fornax cluster galaxies are HI-deficient compared to field galaxies. The kinematics of the cluster galaxies suggests that the HI deficiency may be caused by ram-pressure stripping of galaxies on orbits that pass close to the cluster core.

We also derive the most complete *B*-band Tully–Fisher relation of inclined spiral galaxies in Fornax. A subcluster in the South-West of the main cluster contributes considerably to the scatter. The scatter for galaxies in the main cluster alone is 0.50 mag, which is slightly larger than the intrinsic scatter of 0.4 mag. We use the Tully–Fisher relation to derive a distance modulus of Fornax relative to the Virgo cluster of -0.38 ± 0.14 mag. The galaxies in the subcluster are (1.0 ± 0.5) mag brighter than the galaxies of the main cluster, indicating that they are situated in the foreground. With their mean velocity 95 km s^{-1} higher than that of the main cluster we conclude that the subcluster is falling in to the main Fornax cluster.

Key words: Galaxies: clusters: general – Galaxies: clusters: individual: Fornax – Galaxies: fundamental parameters – Galaxies: general – Radio lines: galaxies

1. Introduction

The nearby Fornax cluster has a high central surface density of galaxies (Ferguson 1989b) although it is not a rich cluster in Abell’s (1956) sense. It forms an intermediate sample suitable for comparison with richer clusters like Virgo (Huchtmeier & Richter 1989a; Cayatte et al. 1994) and Hydra I (McMahon et al. 1992), as well as smaller groups and nearby field galaxies (Huchtmeier & Richter 1988; Marquarding 2000).

In particular, Fornax lies almost opposite in the sky from the well-studied Virgo cluster but at a distance just about equal to it (*e.g.*, Pierce 1989; Bridges et al. 1991; Hamuy et al. 1991; McMillan et al. 1993; see also Table 6.1 in Schröder 1995). A better understanding of the relative distance and the substructuring in both clusters would allow one to disentangle the effects of virgocentric infall from larger-scale motions relative to either one or more distant galaxy aggregates, such as the “great attractor” (Kolatt et al. 1995), or the microwave background radiation reference frame. Fornax has also been used in studies of the extragalactic distance scale (see Freedman et al. 2001, and below).

The HI content of the Fornax cluster galaxies has, heretofore – by virtue of the cluster’s southern declination just beyond the reach of most major northern radio telescopes – not been studied in a comprehensive way (*cf.* Sec. 3 for references). More recent HI surveys of the cluster galaxies include Horellou et al. (1995) and Bureau et al. (1996). Barnes et al. (1997) conducted a shallow blind survey of the inner $8^\circ \times 8^\circ$ of the cluster; a more detailed blind survey of the whole cluster area using the Parkes Multibeam receiver (Staveley-Smith et al. 1996) is currently under way (Vaughn et al. 2000).

Our main motivation in this study was to obtain an improved Tully–Fisher relation for the Fornax cluster (*cf.* Schröder 1995) as well as confirming cluster membership with new HI radial velocities. Our sample included all galaxies listed in the RSA¹ catalogue that lie within 5 degrees from the approximate cluster centre at $\alpha = 03^{\text{h}}35^{\text{m}}$

¹ A Revised Shapley-Ames Catalog of Bright Galaxies (Sandage & Tammann 1981, 1987).

Table 1. Observational parameters of the four runs

run	May/Jun 91	Jan 92	Jun 93	Apr/May 94
system noise temperature	40-45 K	40-45 K	30 K	30 K
channel	1024	2048	2048	2048
bandwidth	10 MHz	8 MHz	32 MHz	32 MHz
channel spacing	4.1 km s ⁻¹	1.7 km s ⁻¹	6.6 km s ⁻¹	13.2 km s ⁻¹
velocity resolution (after smoothing)	9.8 km s ⁻¹	7.9 km s ⁻¹	15.8 km s ⁻¹	15.8 km s ⁻¹

and $\delta = -35.7^\circ$ (basically the position of NGC 1399) and which have a radial velocity less than 2300 km s^{-1} . To this we added those galaxies from the comprehensive catalogue of Fornax cluster galaxies by Ferguson (1989a, hereafter FCC) which he (a) judged to be either certain or possible members, and (b) classified to be of sufficiently late morphological type to suspect a detectable HI content. We also decided to reobserve some of the weaker and less well-determined HI lines already known from the HI catalogue by Huchtmeier & Richter (1989, henceforth HR89). Finally, two possible background galaxies were added to confirm non-membership.

The final sample comprises 66 galaxies of which we detected 37 in HI. The results are presented in Section 3 with the description of the observations given in Section 2. In Section 4 we analyse the distribution of HI content in the cluster galaxies, and in Section 5 we derive the Tully–Fisher relation.

2. Observations

The Parkes 210 ft (64 m) radio telescope was used during several sessions to observe the sample of Fornax galaxies described above. Additionally, several galaxies previously observed in the 21 cm line (*cf.* the HR89 catalogue) were reobserved to improve data quality and to allow a better comparison with previously published data. The first observing run was in late May and early June 1991, a second in January 1992, a third one in June 1993, and a fourth one in late April and early May 1994. Table 1 gives an overview of the observational parameters.

All observations were carried out in the total power mode. 10-minute ON-source observations were preceded by an equal length OFF-source observation at the same declination but 10.5 minutes earlier in right ascension, so as to traverse the same path in geocentric coordinates during both the reference and the signal observation. To avoid having to use too many intra-cluster OFF-source positions, we attempted to use a single OFF-source observation outside the cluster area for several cluster galaxies loosely aligned along a “path” at roughly equal declination and – again – spaced about 10 minutes in right ascension. It should, however, be noted that a number of OFF-source positions were located well within the boundaries of the Fornax cluster.

For each galaxy such ON/OFF-observations have been repeated until the signal was unambiguous (in case of interferences) and the signal-to-noise was at least 3–5.

The dual-channel AT 21 cm receiver used in 1991 and 1992 had a system noise temperature of order 40–45 K. In 1993 and 1994 a new receiver with a system noise temperature of about 30 K was used. In 1991 a 1024-channel autocorrelator served as the backend. It was split into two banks of 512 channels each which detected the two independent polarisations. A bandwidth of 10 MHz ($\approx 2100 \text{ km s}^{-1}$) with a central frequency corresponding to a heliocentric radial velocity of 1300 km s^{-1} was used for all galaxies regardless of the availability of a known radial velocity. Beginning in 1992 a new autocorrelator (technically quite similar to the correlators in use at the Australia Telescope Compact Array in Narrabri) was available with 2048 channels, which were also split into 2 banks of 1024 channels and 8 MHz bandwidth each. Once, in January 1992, this new autocorrelator suffered a processor failure and data for a single 24-hour period were again taken with the old autocorrelator.

The autocorrelator setup was changed in 1993 to accommodate other parallel programs to be reported elsewhere. The bandwidth was changed to 32 MHz with 1024 channels in each bank. In 1994 we used a split into 4 banks of 512 channels each with an IF offset of 25 MHz for the third and fourth bank of the autocorrelator to also cover a higher velocity range out to 12000 km s^{-1} . This information came basically free of cost, since banks 1 and 3 as well as 2 and 4 were fed by the same polarisation output from the receiver, *i.e.*, would have differed only by the quantization noise which was practically undetectable. No serendipitous signals, however, showed up in this higher velocity range for Fornax galaxies.

In all cases the two different polarisations were averaged during data reduction. Fitted spectral baselines consisting of a polynomial of moderate order added to a sine function with a period equal to that of the standing wave pattern of the Parkes telescope (5.8 MHz) were subtracted to form the final spectra.

The online control program automatically corrected for the zenith angle dependence of the telescope sensitivity. The primary flux calibration was obtained by measuring standard sources from the Parkes catalogue (Wright

& Otrupcek 1990) at the beginning of each observing session; it was stable to within $\approx 10\%$. As an added check of system performance secondary HI flux calibrators chosen from the new compilation of HI data for RSA galaxies by Richter et al. (1994, priv. comm.) were observed from time to time. Based on those data the internal consistency of the flux scale is indeed judged to be better than 15%.

3. Results

We present our results in this section as a table of the HI measurements, notes on individual galaxies and a comparison with other measurements. The HI spectra of the detected galaxies are shown in the Appendix. It should be noted that the number of Hanning smoothing operations for the displayed spectra varies from 1 to 4 depending on the overall signal-to-noise ratio.

3.1. The new HI Data

In Table 2 we present the averaged data of the four runs (in general a weighted mean) together with some parameters from the FCC. The Table columns are as follows.

Col. 1a: Galaxy identification according to the FCC.

Col. 1b: Other galaxy identification: NGC, IC, ESO in this order of preference.

Col. 2: Coordinates in J2000 equinox.

Col. 3: Morphological type from the FCC. Where the galaxy was not in FCC, RC3² values have been taken.

Col. 4: *B*-band magnitude from the FCC. Where the galaxy was not in FCC, RC3 values have been taken.

Col. 5: Decimal logarithm of the diameter, $\log D$, in units of 0.1 at the 26.5th *B*-band isophote from the FCC. For non-FCC members we have taken $\log D_{25}$ from the RC3 and added 0.05, which is the mean difference between FCC and RC3 values.

Col. 6: Axial ratios, $\log R$, from Lauberts & Valentijn (1989). For galaxies with no entry we have taken the axial ratios from Paturel et al. (2000; cf. the LEDA³ database). They are indicated with a superscript *a*. For one galaxy (superscript *b*) the axial ratio comes from MacGillivray et al. (1988), and for two galaxies no axial ratios could be found in the literature and our own measurements are given (superscript *c*).

Col. 7a: Weighted mean heliocentric HI radial velocity in km s^{-1} taken at the midpoint of the HI profile at the 20% level. The optical convention $v = c(\lambda - \lambda_0)/\lambda_0$ is used.

Col. 7b: Error of the radial velocity, calculated according to Fouqué et al. (1990): $\sigma(v) = 4R^{0.5}P^{0.5}s^{-1}$ where R is the resolution in km s^{-1} (1.2 times the channel spacing), P is the steepness of the edges of the profile

($P = (\Delta v_{20} - \Delta v_{50})/2$), s is the signal-to-noise, i.e., peak S_h over rms noise level.

Col. 8a: Velocity width in km s^{-1} of the HI profile measured at the 50% level of the peak intensity, Δv_{50} , corrected for instrumental broadening: no correction for $0 < R \leq 8 \text{ km s}^{-1}$, -3 km s^{-1} for $8 < R \leq 16 \text{ km s}^{-1}$, -5 km s^{-1} for $16 < R \leq 32 \text{ km s}^{-1}$, -7 km s^{-1} for $32 < R$. The smallest line width of the four runs has been selected (since there is no known mechanism that would artificially decrease the line width).

Col. 8b: Velocity width in km s^{-1} of the HI profile measured at the 25% level of the peak intensity, Δv_{25} , corrected for instrumental broadening (cf. Col. 6a).

Col. 8c: Velocity width in km s^{-1} of the HI profile measured at the 20% level of the peak intensity, Δv_{20} , corrected for instrumental broadening (cf. Col. 6a).

Col. 9a: Weighted mean HI flux, which is the line integral in Jy km s^{-1} , uncorrected for finite beam size.

Col. 9b: The error of the HI flux is the combined error for the measurement of the profile and the flux calibration: $\sigma = (\sigma^2(A) + (0.1A)^2)^{0.5}$ with $\sigma(A) = 5R^{0.5}A^{0.5}h^{0.5}s^{-1}$ (according to Fouqué et al. 1990) where A is the line integral and the other parameters as described for Col. 5b.

Col. 10: Weighted mean HI peak flux S_h in Jy.

Col. 11: Calculated HI mass in $10^8 d_{20}^2 M_\odot$ using $M_{HI} = 2.365 \times 10^5 d^2 S = 948 \times 10^5 S d_{20}^2 M_\odot$, where S is the HI flux from Col. 9a, and the distance is $d = 20 d_{20} \text{ Mpc}$ (cf. Sec. 4.3). No HI masses were computed for background detections.

Col. 12: The rms noise level S_{rms} over the region used to fit a baseline, in 10^{-3} Jy . The smallest values of the four runs are given here.

Col. 13: The runs when the galaxy was observed.

Col. 14: Notes: the search interval for the possible background galaxy FCCB37 is given. A star denotes interferences in the spectra which could have prevented us from detecting the line. It is indicated at the bottom of the table if a velocity is known for that object. A hash sign indicates if the smallest line width has been discarded because of either a very low S/N of about three or a large correction for instrumental broadening ($\geq 7 \text{ km s}^{-1}$). A dagger means that the diameter has been derived from RC3 values.

3.2. Notes on individual objects

FCC2 was classified as a cluster member by Ferguson (1989a) but we have shown it to be a background spiral at $v = 4540 \text{ km s}^{-1}$.

FCC35 shows two unusual-looking peaks. It was confirmed to be at 1800 km s^{-1} by follow-up observations made at Parkes by Staveley-Smith (1994, priv. comm.) and has more recently been observed with the ATCA (Australia Telescope Compact Array) by Putman et al. (1998), who found that one of the peaks is caused by a

² Third Reference Catalogue of Bright Galaxies (deVaucouleurs et al. 1991).

³ Lyon-Meudon Extragalactic Database; <http://leda.univ-lyon1.fr>.

nearby intergalactic HI cloud, and the other, as presented here, by the galaxy proper.

FCC 121 (NGC 1365) was used as an intra-cluster check of system performance by separately reducing each 10-minute observation, in each polarisation band, of this galaxy. Note that only the final averaged data are given in the table.

FCC 306 lies in the beam of FCC 308 and has been confirmed in a FLAIR observation with $v = 915 \pm 15 \text{ km s}^{-1}$ using emission lines (Schröder 1995).

FCC 338 was classified as S0 in FCC but seems more likely to be an Sab as given in RC3.

FCC B74, the brightest background spiral galaxy in Ferguson's classifications, has been confirmed with $v = 4147 \text{ km s}^{-1}$.

3.3. Comparison with earlier data

Galaxies in the Fornax cluster have been previously surveyed for HI content by – among others – Fouqué et al. (1990), Mathewson et al. (1992), Horellou et al. (1995), Bureau et al. (1996), and Barnes et al. (1997). For a detailed listing of references before 1989 the reader is referred to the HR89 catalogue.

In general, the agreement of our HI radial velocities with published values is excellent with deviations never exceeding the stated – usually internal – errors. However, HI fluxes vary considerably with differences more often than not larger than the quoted relative errors (usually 10–15%, *cf.* Sec. 2). Varying signal-to-noise ratios for the weaker HI spectra have a significant impact also on the measured HI line widths. During our own observations, we therefore attempted to improve upon the weaker signals rather than observing a larger number of objects. Yet, not all line widths are of the same quality.

We have compared the line widths with published data in the literature: Bottinelli et al. (1990), Mathewson et al. (1992), and Bureau et al. (1996) give HI line widths for Fornax galaxies. The agreement is within the errors for both 20% and 50% line widths except in the case of the 20% line width of Bureau et al. which show a mean deviation of $(10 \pm 3) \text{ km s}^{-1}$ (for 18 galaxies in common). The comparison with the other sources indicates that their line widths are too broad by $\sim 7 \text{ km s}^{-1}$ (after correction for instrumental broadening).

4. The HI content of the Fornax cluster

In this section we examine the distribution of HI in the Fornax cluster based on our observations. We first describe the galaxies detected in HI and then compare their distribution with that of the galaxies not detected before comparing their HI masses with galaxies in other environments.

4.1. The HI detections

Our data represent some of the deepest observations ever made of Fornax cluster galaxies in HI. We detected 37 of the 66 galaxies, 12 of them for the first time (and two being background galaxies). Figure 1 shows the morphological types of our sample (with the numerical coding as in RC3): non-detections are represented through the standard deviation of the noise (rms) of their HI spectra (open circles), whereas the peak flux is given for the detected galaxies. Only a few spiral galaxies were not detected, in particular three out of four Sa galaxies. Four of the undetected late-type galaxies are affected by interference at $v \simeq 1250 \text{ km s}^{-1}$, which may have prevented the detection of the galaxy in its vicinity (no velocities are known from the literature). The fifth galaxy (FCC 299) has an optical velocity of $(2051 \pm 9) \text{ km s}^{-1}$ (Schröder 1995). A marginal detection at this velocity is possible but would require at least two more hours of observation to be confirmed.

No elliptical or S0 galaxies ($T = -2$) were detected. We have assigned $T = -5$ to the dwarf spheroidal and Im/dE galaxies since these classifications indicate early type galaxies.

4.2. The distribution of HI detections

In the following discussions we have not included the two galaxies with HI detected at high velocity (FCC 2 and FCC B74) as they are not cluster members.

The present paper gives the most comprehensive list of HI detections in the Fornax cluster to date. In Fig. 2 we show the distribution of FCC galaxies in the sky, with the HI detections as filled circles and the non-detections as open circles. Note that our sample includes four galaxies

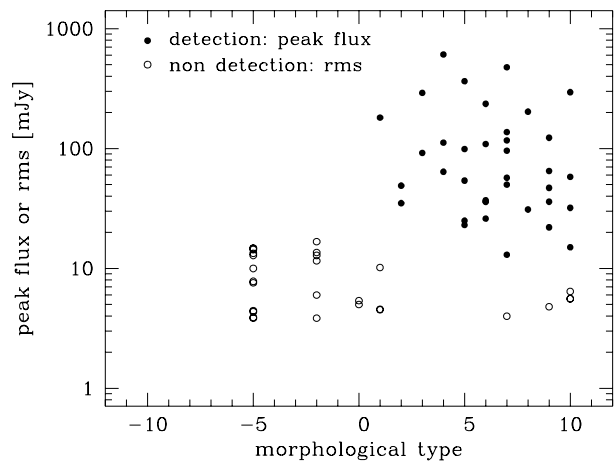


Fig. 1. Distribution of morphological type for detections (filled circles: peak flux is given) and non-detections (open circles), which are represented through the rms of the HI spectrum.

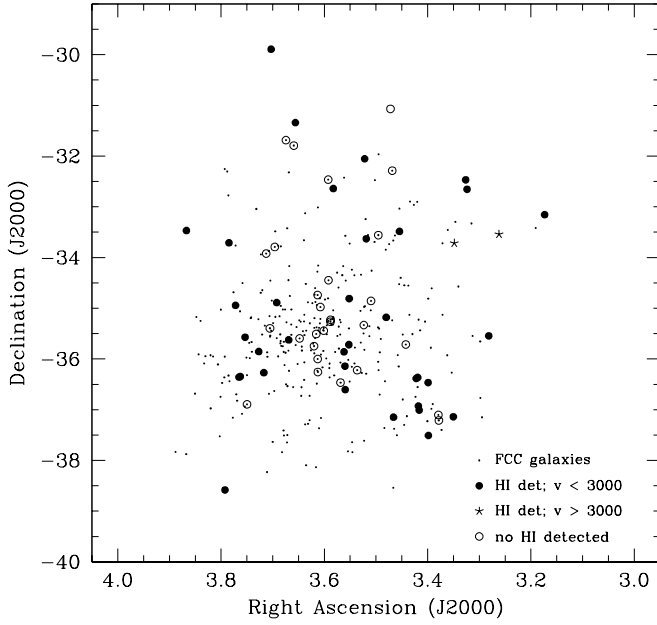


Fig. 2. The distribution of FCC galaxies (dots), HI detections of the present work (filled circles) and non-detections (open circles) in J2000 coordinates. Stars indicate HI detections of background galaxies.

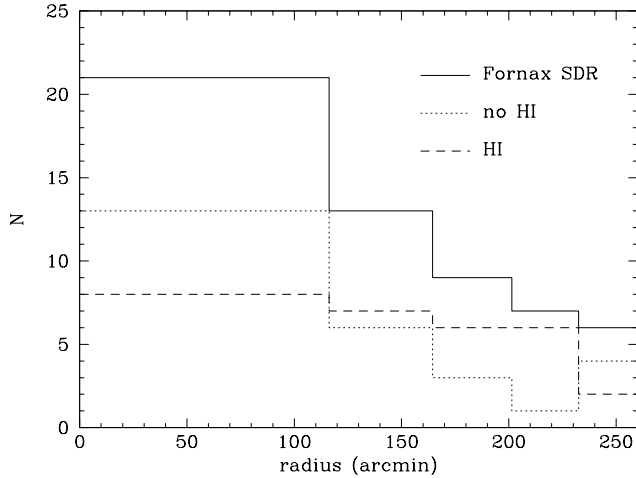


Fig. 3. The distribution of our total sample, detections (dashed line) and non-detections (dotted line) in equal area bins as a function of distance from the cluster centre.

outside the FCC as well as three background galaxies of which two are not in the FCC main catalogue. To quantify we plot in Fig. 3 the numbers of galaxies in radial annuli of equal area for the total sample and the galaxies with and without HI detections.

Both Figures 2 and 3 show that the galaxies with HI detections are evenly distributed across the cluster, whereas those without any detected HI are much more concentrated towards the cluster centre. This is to a large

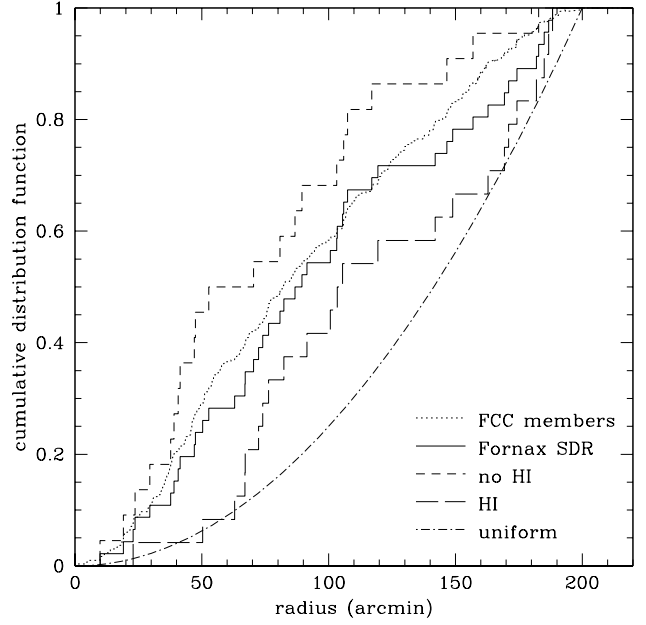


Fig. 4. Cumulative radial distribution of our total sample (solid line) compared to the distribution of all cluster members in the optical FCC sample (dotted line). The subsamples of our galaxies with and without any detected HI are indicated by long and short dashed lines respectively. A uniform, constant-density distribution is also shown for comparison.

extent a reflection of the usual density-morphology relation: the ratio of early to late-type galaxies increases rapidly towards the cluster core. In Fig. 3 the distribution of galaxies with detected HI is consistent with a constant surface density as though these galaxies were not aware of the cluster, although this is partly due to the binning: see the cumulative distribution in Fig. 4.

In Fig. 4 we plot the same data as cumulative distribution functions, also including cluster members listed in the optical FCC catalogue. We can now assess the significance of the difference in the distributions. The radial distribution of our total sample is not significantly different from that of the FCC members: they differ at a Kolmogorov-Smirnov (KS) significance of only 15%. There is a significant difference in the radial distributions of the HI and non-HI samples: they differ at a KS significance of 97% with the non-detected galaxies being much more concentrated towards the cluster centre. Interestingly, the distribution of the HI detected galaxies is also more centrally concentrated than a uniform distribution (dash-dotted curve in Fig. 4) at a KS significance of 94%. The HI-rich galaxies are not distributed as a uniform sheet but clearly show signs of being concentrated towards the cluster although at larger radii than the non-detected galaxies.

We also compared the velocity distribution of the cluster galaxies detected in HI with published velocities of the

other cluster members in our sample. The 35 cluster galaxies detected in HI have a mean velocity of $1480 \pm 60 \text{ km s}^{-1}$ and the 26 members not detected in HI with published velocities have a mean velocity of $1460 \pm 70 \text{ km s}^{-1}$. There is no significant difference in these velocity distributions.

4.3. The HI masses

Estimates of the HI mass depend on the cluster distance, which is currently under discussion. There are Cepheid distances available for three Fornax galaxies: NGC 1365 at 18.6 Mpc (Madore et al. 1999), NGC 1326A at 18.7 Mpc (Prosser et al. 1999), and NGC 1425 at 22.2 Mpc (Mould et al. 2000). Drinkwater et al. (2001a) have shown that NGC 1326A is part of a subcluster in front of the main cluster (see Section 5) and they also argue that NGC 1365 is in front of the cluster core. They therefore propose – as did Mould et al. (2000) – that the mean of the three distances, 20 Mpc, be adopted for the Fornax cluster. We note that there is still no consensus in the literature on this matter, and for this paper we parameterise the distance as $d = 20d_{20}$ Mpc.

The HI masses for our galaxies are calculated using $M_{\text{HI}} = 2.37 \times 10^5 d^2 S = 948 \times 10^5 S d_{20}^2 M_{\odot}$, where S is the HI flux integral in Jy km s^{-1} . These distance-parameterised masses are listed in Table 2 in units of $d_{20}^2 M_{\odot}$.

NGC 1365 ($T=4$) has the largest HI mass in Fornax and is one of the most HI-massive galaxies known. The second most HI-massive galaxy in Fornax, NGC 1326B ($T=7$), is one member of an interacting pair. Its HI mass-to-light ratio is extremely large, presumably due to its interactions (*cf.* Fig. 5). Its companion, NGC 1326A ($T=5$), shows no unusual parameters.

NGC 1316C has the lowest HI mass for the Sd galaxies. It is a close neighbour of FCC 35 ($T=9$) which is associated with an HI cloud (Putman et al. 1998). This HI cloud may have been stripped from NGC 1316C by a close encounter with FCC 35, which has an HI mass consistent with its morphological type.

The distance-independent HI mass-to-blue light ratio M_{HI}/L_B is shown in the upper panel of Fig. 5 in logarithmic scale. We have binned the data in pairs of morphological types for better statistics (1–2, 3–4, 5–6, 9–10) and calculated the mean. The result is shown in the lower panel of Fig. 5. NGC 1326B with its extreme M_{HI}/L_B has been excluded from this mean.

In comparison we show the means of galaxies in the Virgo cluster (triangles), as derived from data obtained with the Arecibo telescope (Helou et al. 1981; Helou et al. 1984; Hoffman et al. 1987; Hoffman et al. 1989; for simplicity we shall call this the HHC data, as in Helou, Hoffman and collaborators). For the calculation of the mean we have again excluded an unusually large M_{HI}/L_B (for $T=3$) in this data-set. Despite the larger errors for the Fornax sample (due to small sample statistics) we can see

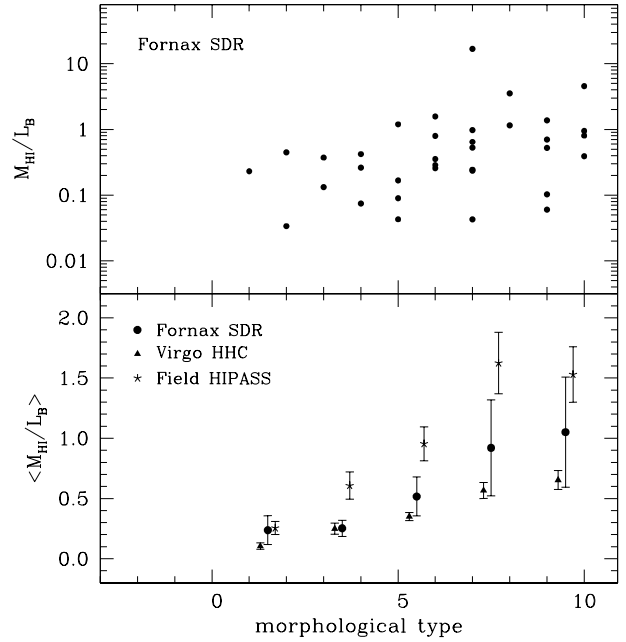


Fig. 5. The HI mass-to-blue light ratio versus morphological type for our sample. The upper panel shows the distribution of the sample in logarithmic scale, the lower panel shows the binned data in comparison with the Virgo cluster (triangles) and with the field (stars). For clarification the points are slightly offset in types.

that the Virgo galaxies, well-known for their HI depletion, have systematically lower M_{HI}/L_B ratios. The mean M_{HI}/L_B for the Fornax sample is 0.68 ± 0.15 whereas that of the Virgo sample is 0.45 ± 0.03 . The means differ at the 85% confidence level according to the T-test.

Finally, we also show the means from data obtained in the HI Parkes All-Sky Survey (HIPASS) of bright field galaxies in the southern hemisphere (Marquarding 2000; see also Staveley-Smith et al. 1996 for a description of the survey). The HI selected field galaxies (indicated with stars) show systematically larger M_{HI}/L_B ratios than the galaxies in either cluster. The mean M_{HI}/L_B for the field sample is 1.15 ± 0.10 which is larger than the Fornax value at the 98% confidence level and larger than the Virgo value at a confidence level greater than 99.9% (both according to the T-test).

Galactic extinction corrections have been applied to the HIPASS sample; in case of Fornax and Virgo we assume the Galactic extinction to be zero or negligible. Since the HIPASS sample does not have inclinations for all galaxies we have not corrected the blue luminosities for any of the samples for internal absorption. A correction for internal absorption will lower the mean value of M_{HI}/L_B . The HIPASS sample is limited by peak flux and therefore biased against largely inclined galaxies. However, the correction in this case would be smaller than for the cluster samples with their more evenly distributed inclinations

and the difference between field and cluster galaxies will be increased.

4.4. HI deficiency

Solanes et al. (1996, hereafter SGH) have shown that the HI content of isolated spiral galaxies not only depends on morphological type but also shows a tight linear relation with the linear optical diameter. We can therefore compare the actual observed HI mass as derived from our HI fluxes with the expected value for a galaxy unaffected by environmental conditions and of the same diameter and morphological type. Using the tabulated coefficients for the expectation value of the logarithm of the HI mass, $\log \widehat{M}(T, D)$, from SGH, we have calculated the HI deficiencies for our galaxies as

$$HI_{def} = \log \widehat{M}_{HI}(T^{obs}, D_{opt}^{obs}) - \log M_{HI}^{obs},$$

where the diameters are given in kpc and the HI masses in solar units. We have used the diameters from the FCC (measured at the 26.5th isophote), and corrected RC3 diameters for 3 galaxies outside of the FCC by adding the mean difference of 0.05. Since SGH have used UGC⁴ diameters, we have then adjusted the conversion given by Horellou et al. (1995) to compute UGC from our FCC diameters:

$$\log(D_{UGC} + 0.3) = 1.0173 \log D_{25}.$$

Because of the additional correction for diameter dependence, we would expect the HI deficiencies to have a smaller internal scatter and be a better indicator for variations in HI content than the M_{HI}/L_B values. However, in addition to the (sometimes large) errors in observed HI flux, diameter and morphological type, both the HI mass and the linear diameters are distance dependent, which increases the scatter in the HI deficiencies again. While the same distance can be used for a small nearby cluster as Fornax, the distances to the field galaxies used for the expectation value by SGH depend on the Hubble constant and show errors due to peculiar velocities. Solanes et al. (2001) therefore emphasise that HI deficiencies are only meaningful in a statistical sense.

Expectation values of HI masses are only well determined for types $T=1-5$. As indicated by Solanes et al. (2001), we have calculated the expectation values of HI masses for the later types ($T=6-10$) using the coefficients for $T=5$. Though the variation in the coefficients with morphological type are small (*cf.* Haynes & Giovanelli 1984), we want to emphasise that HI deficiencies for types (much) later than 6 are less reliable.

Figure 6 shows the HI deficiencies of all our Fornax galaxies with HI measurements. The scatter is large and the number of galaxies for each morphological type is small. We have therefore derived a mean HI deficiency

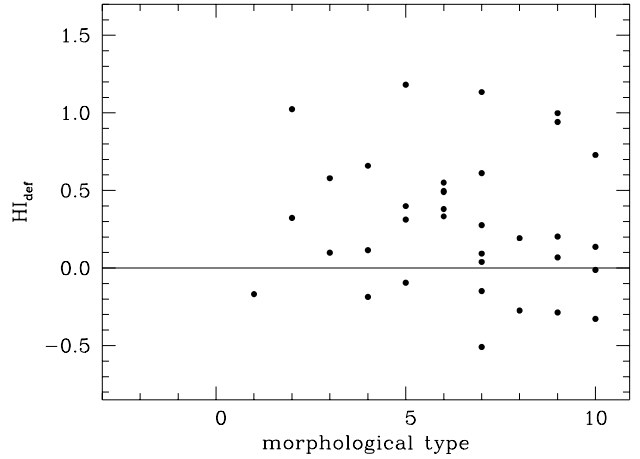


Fig. 6. The HI deficiency parameter versus morphological type for our sample. The expected HI masses for galaxies with $T \geq 6$ were calculated using the relationship for galaxies with $T=5$.

for the types $T=1-5$ together: $\langle HI_{def} \rangle = 0.35 \pm 0.13$. Including galaxies with $T=6$, we find the similar value of $\langle HI_{def} \rangle = 0.38 \pm 0.09$. If we assume that the deficiency is reliably defined for the later types as well, we find $\langle HI_{def} \rangle = 0.30 \pm 0.07$, which is close to the other values. These results show a significant if moderate HI deficiency for the Fornax cluster, independent of our M_{HI}/L_B calculations above. Our deficiency value is consistent with that of Horellou et al. (1995) who derived a deficiency of 0.43 ± 0.55 , with a much larger uncertainty.

We have calculated HI deficiencies for the HIPASS sample as well, using RC3 diameters where available (for 106 out of 136 galaxies). The mean deficiencies for all types together as well as for each type separately are consistent with zero (*e.g.*, 0.05 ± 0.03 for $T=1-6$), indicating that the sample, though HI selected and not optically selected, is representative for the field. The scatter for $T=1-6$ is 0.24 and comparable to the scatter of 0.23 quoted by SGH for their field galaxies.

4.5. Discussion

Environmental effects on the HI content of spiral galaxies have been discussed at length in the literature (*e.g.*, Solanes et al. 2001; Abadi et al. 1999; van Gorkom 1996; Giovanelli & Haynes 1985; and many others). There are two main mechanisms that can strip galaxies of their gas content: ram-pressure stripping by interaction with hot intra-cluster gas, and tidal interactions with other galaxies. The second mechanism can also strip stars off the outer parts of a galaxy. Other mechanisms are viscous stripping and thermal conduction. Rich galaxy clusters, like Virgo (Solanes et al. 2001; Cayatte et al. 1994; Guhathakurta et al. 1988; Hoffman et al. 1988; to name only a few) or Coma (Bravo-Alfaro et al. 2000; Bothun

⁴ Uppsala General Catalog of Galaxies (Nilson 1973).

et al. 1984) have large X-ray luminosities, and galaxies in the inner part of the clusters show definite signs of loss of HI gas due to ram-pressure stripping.

Fornax is a small cluster but with a high central galaxy density. Its X-ray luminosity is much lower than that of the Virgo cluster (about 2 orders of magnitude) with a significant detection only in the core of the cluster (Killeen & Bicknell 1988; Jones et al. 1997). Within the core region however (a projected radius of about 20 arcmin) the mean gas density is of order 10^{-3}cm^{-3} (Jones et al.) so pressure stripping will be effective with timescales of 10^9 years according to the conservative estimates of Ferguson & Binggeli (1994). There is also direct evidence for stripping in some of the central Fornax galaxies from their morphologies, e.g. NGC 1404 (Jones et al. 1997). The effect of pressure stripping is harder to calculate at larger radii, but it is presumably much lower. In a large sample of galaxies from different clusters (most well-outside the core region), Solanes et al. (2001) found no apparent relationship between (strong) X-ray luminosity and HI deficiency in individual galaxies. (However the fraction of gaseous late-type spirals in the centre of rich clusters may be reduced in favour of lenticulars that have no or only little gas content.)

Our Fornax data demonstrate a non-zero HI deficiency parameter as well as a mean M_{HI}/L_B ratio significantly lower than that found for a sample of field galaxies. This is for a sample of galaxies that extends well beyond the core where we might expect pressure stripping to be important. This result appears to conflict with previous non-detections of any *strong* HI deficiency in Fornax (Horellou et al. 1995, and Bureau et al. 1996). In the former case the sample actually measured was very small (only 6 new measurements of cluster galaxies), which resulted in a large uncertainty, and they were mostly earlier types where the depletion is weaker. In the case of the Bureau et al. result the conclusion was based on a comparison with galaxies in the Ursa Major cluster. We note that the Fornax cluster is not significantly denser than Ursa Major if the central core region is excluded and that we might therefore expect them to have similar HI deficiencies. Our use of a large sample and our comparison with a genuine field sample from the HIPASS data (Marquarding 2000) has allowed us to detect the HI deficiency in the Fornax cluster.

As we describe above, a number of mechanisms have been proposed that could explain the HI deficiency of Fornax cluster galaxies. Most of the galaxies we detected in HI are well beyond the cluster core where the pressure of the hot X-ray gas is high enough for ram-pressure stripping. However, as discussed by Solanes et al. (2001), this mechanism is still viable if the galaxies are on radial orbits in the cluster. Our sample is too small for a detailed analysis of the orbits, but we can make a simple comparison of the kinematics of the HI-deficient galaxies ($\text{HI}_{\text{def}} > 0.3$, $n=17$) with the rest of the HI detected

galaxies. The HI-deficient galaxies have a smaller velocity dispersion ($247 \pm 44 \text{ km s}^{-1}$) than the other galaxies ($391 \pm 67 \text{ km s}^{-1}$) with the difference significant at the 93% confidence level. Splitting the sample according to M_{HI}/L_B ratio gives very similar results. This difference in velocity dispersions is consistent with the deficient galaxies having more radial orbits than the other galaxies as was shown for a composite cluster sample by Solanes et al. (2001). One further process that will contribute to HI depletion is the conversion of neutral gas into stars. Our optical measurements (Drinkwater et al. 2001b) have shown that there is an excess of star formation in Fornax cluster galaxies at similar distances to most of our HI detections. Although the corresponding gas depletion timescales are long (of order 10^{10} years), this does show that the cluster environment can influence the gas content of galaxies even at these large distances.

5. The Tully – Fisher relation

During our observing programme we observed all spiral galaxies in the FCC with long integration times. In combination with the multi-colour multi-aperture data obtained by one of us (Schröder & Visvanathan 1996; Schröder 1995) this comprehensive sample enables us to establish the Tully – Fisher relation for all inclined spiral galaxies ($i \geq 45^\circ$, $1 \leq T \leq 9$) in the Fornax cluster. We have taken the parameters as well as the corrections as described in Schröder (1995): morphological types are from the FCC, axial ratios are mainly from Lauberts & Valentijn (1989, *cf.* notes to Table 2), q_0 to calculate inclinations are from Heidmann et al. (1971), and internal absorptions have been corrected according to the RC3. We have taken the 20% line widths from Tab. 2 (which are corrected for instrumental broadening), and applied a correction for z-motion and turbulences of -12.6 km s^{-1} as explained in Richter & Huchtmeier (1984). For the Tully – Fisher relation we use the maximum rotational velocity $V_M = \Delta v_{20}^c (2 \sin i)^{-1}$. Adopting a slope of -6.50 from the Virgo cluster (Schröder 1995) where we have better statistics, we find

$$B_T^{2,i}(F) = -6.50 \cdot [\log V_M - 2.0] + (12.56 \pm 0.18)$$

with a scatter of 0.84 mag.

Excluding the faintest galaxy from the relation, FCC 306 (*cf.* Fig. 7), we find a scatter of 0.71, which is considerably smaller. No obvious explanation for such a deviation could be found: This Sm galaxy has a strong HI signal, and the velocity has been confirmed with an optical measurement (Schröder 1995). Its 20%-width is possibly smaller by $\sim 15 \text{ km s}^{-1}$ (Waugh, priv. comm., using HIPASS data) which would result in a scatter of 0.81. Its HI mass and M_{HI}/L_B is consistent with other galaxies of this type. The optical data is good (four apertures covering a large range in radius of the galaxy) and the total magnitude is comparable to the magnitude given by

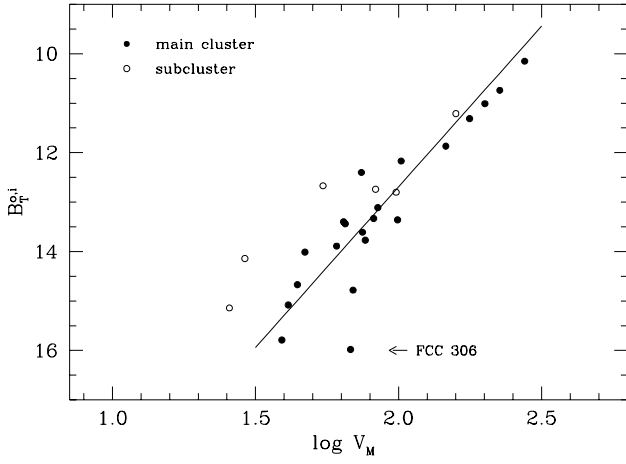


Fig. 7. The Tully – Fisher relation for the Fornax cluster. Open circles denote galaxies which seem to belong to a subcluster. The linear regression is derived for the main cluster only and without FCC 306.

Lauberts & Valentijn (1989). The axial ratio is confirmed by Loveday (1996). However, we believe that its unusually large effect on the scatter of the Tully – Fisher relation justifies sufficiently its exclusion from here on from the relation. We assume that a combination of errors in the various parameters accounts for its unusual high deviation from the Tully – Fisher relation. However, another explanation would be that this galaxy lies off the main Tully – Fisher relation because it actually lies behind the main cluster and is falling into it. This argument is supported by the very compact morphology of FCC 306: it has the smallest angular size and highest surface brightness of the star-forming dwarfs in the sample of Drinkwater et al. (2001b).

Due to its small velocity dispersion the Fornax cluster has so far been assumed to have no substructure. However, Drinkwater et al. (2001a) have analysed the dynamics of the cluster and find definite evidence for a subcluster in the South West of the cluster, centred on Fornax A (NGC 1316). In fact, a slightly enhanced galaxy density in this region can also be seen in Fig. 16 of the FCC. If we exclude the galaxies in this subcluster from the Tully – Fisher relation we obtain

$$B_T^{o,i}(F) = -6.50 \cdot [\log V_M - 2.0] + (12.69 \pm 0.12),$$

as shown in Fig. 7, with a scatter of 0.50. The scatter is considerably smaller than before and comparable to the intrinsic scatter, which is about 0.4 (*cf.* Sakai et al. 2000 find 0.43 for near-by galaxies with Cepheid distances).

We have not attempted to derive a Tully – Fisher relation of the subcluster alone since only six galaxies therein are useful for the Tully – Fisher relation. Furthermore, one of these has unusual HI masses due to interactions (NGC 1316C, *cf.* Sec. 4). However, in the mean they are

(1.0 ± 0.5) mag brighter than the main cluster, indicating that the subcluster lies in the foreground of Fornax (which is also supported by the lower Cepheid distance of NGC 1326A, 18.7 Mpc, in the subcluster). In combination with its slightly larger mean velocity of 1583 km s^{-1} (as compared to 1478 km s^{-1} for the main cluster, Drinkwater et al. 2001a) we now have a three-dimensional picture of the subcluster in the foreground falling into the main cluster. The high rate of HI detection in the subcluster (see Fig. 2) suggests that it is falling into the main cluster for the first time. This is consistent with the slightly lower HI deficiency (0.2 ± 0.2) we measure for the subcluster galaxies compared to the rest of the cluster (0.44 ± 0.10) .

The Tully – Fisher relation for the main cluster can be used to derive a relative distance to the Virgo cluster as shown by Schröder (1995). Using the same parameters and corrections where possible (see description above; morphological types and axial ratios were taken from the VCC⁵, HI line widths from Bottinelli et al. 1990) we find

$$B_T^{o,i}(V) = -(6.50 \pm 0.36) \cdot [\log V_M - 2.0] + (13.07 \pm 0.07)$$

for Virgo, with a scatter of 0.64 mag. This relation includes all galaxies classified as members of the Virgo cluster proper (Binggeli et al. 1993). We find a relative distance of -0.38 ± 0.14 mag with the Fornax cluster being closer. This is consistent with other Tully – Fisher distances between Fornax and Virgo (Bureau et al. (1996): -0.06 ± 0.15 ; Aaronson et al. (1989): -0.25 ± 0.23 ; Visvanathan (1983): -0.20 ± 0.18), contrary to some other distance measurements that place Fornax further away (*e.g.*, McMillan et al. (1993): 0.24 ± 0.10 , using the planetary nebulae luminosity function). The relative distance measurements found in the literature vary from -0.5 mag to $+0.4$ mag (see Tab. 6.1 in Schröder 1995; Tab. 3 in Bureau et al. 1996). However, many methods use only a small sample of galaxies (*e.g.*, type Ia supernovae, surface brightness fluctuations, planetary nebulae luminosity functions) where the cluster centres are less well defined.

The Tully – Fisher relation of the spatially more confined Virgo subcluster B with 20 galaxies shows a smaller scatter of 0.46, similar to the one of the Fornax cluster galaxies and of the calibrators. This agrees well with the velocity dispersion of the B cluster being significantly smaller than that of the whole Virgo cluster (499 km s^{-1} versus 699 km s^{-1} , see Binggeli et al. 1993). We find that the local intercept is fainter (13.21 ± 0.11) and the relative distance larger: -0.52 ± 0.16 mag.

6. Conclusion

In this paper we have presented deep HI observations of all spiral galaxies as well as bright early-type galaxies in the FCC. Two late-type spiral galaxies and three irregulars were not detected, possibly because of an interference at

⁵ Virgo Cluster Catalog (Binggeli et al. 1985).

$v \simeq 1250 \text{ km s}^{-1}$. Only one out of four Sa galaxies was detected, and none of the S0/a galaxies and galaxies of earlier morphological types.

The distribution of galaxies with HI in the Fornax cluster differs significantly from the more centrally concentrated distribution of non-HI detections, as expected from the density-morphology relation. Even the HI-rich galaxies are more centrally concentrated around the cluster than a random distribution: this shows that they are aware of the cluster potential. However, there is no significant difference in the velocity distribution of the two samples.

The mean M_{HI}/L_B binned by morphological type of the Fornax galaxies is between those of the Virgo galaxies and of galaxies in the field indicating a modest but significant HI depletion: the mean M_{HI}/L_B is $60 \pm 13\%$ the value for a comparison sample of field galaxies. In addition, the HI deficiency parameter, as introduced by Solanes et al. (1996), is 0.38 ± 0.09 , which is significantly greater than zero. There is some indication from the kinematics of the galaxies that this HI depletion is caused by ram-pressure stripping of galaxies which are on orbits that pass closer to the cluster core. In addition, optical observations show evidence of enhanced star formation in galaxies in these outer parts of the cluster which will use up some of the gas.

We have calculated the B -band Tully–Fisher relation for the Fornax cluster from our data and obtain a good fit for the main cluster with a scatter of 0.50 mag. The relative distance to the Virgo cluster is -0.38 ± 0.14 mag with the Fornax cluster being closer. The Tully–Fisher relation confirms the existence of a subcluster in the South-West of the main cluster, centred on NGC 1316 (Fornax A). The subcluster galaxies are almost one magnitude brighter than the main cluster. Combined with their higher mean velocity and the higher HI detection rate, this indicates that the subcluster lies in the foreground and is currently falling into the cluster for the first time.

Acknowledgements. We thank the staff at the Parkes Observatory, in particular Euan Troop, for making our stays at the telescope very pleasant and productive. Several people helped us in conducting the observations at the Parkes telescope, notably M.G. McMaster (STScI), R. Otrupcek (ATNF), R.C. Kraan-Korteweg (Univ. of Guanajuato), and P. Henning (Univ. of New Mexico). We are very grateful to M. Waugh and M. Marquarding for making some HIPASS measurements available prior to publication, and to M. Zwaan for helpful discussions. We wish to thank the referee of this paper for detailed comments which greatly improved the presentation of this work. A. S. gratefully acknowledges financial support from the European Marie Curie Fellowship Grant.

References

- Aaronson, M., Bothun, G.D., et al., 1989, ApJ 338, 654
- Abadi, M.G., Moore, B., Bower, R.G., 1999, MNRAS 308, 947
- Abell, G.O., 1958, ApJS 3, 211
- Barnes, D.G., Staveley-Smith, L., Webster, R.L., Walsh, W., 1997, MNRAS 288, 307
- Binggeli, B., Sandage, A., Tammann, G.A., 1985, AJ 90, 1681 (VCC)
- Binggeli, B., Popescu, C., Tammann, G.A., 1993, A&AS 98, 275
- Bothun, G.D., Schommer, R.A., Sullivan, W.T., 1984, AJ 89, 466
- Bottinelli, L., Gouguenheim, L., Fouqué, P., Paturel, G., 1990, A&AS 82, 391
- Bravo-Alfaro, H., Cayatte, V., van Gorkom, J.H., Balkowski, C., 2000, AJ 119, 580
- Bridges, T.J., Hanes, D.A., Harris, W.E., 1991, AJ 101, 469
- Bureau, M., Mould, J.R., Staveley-Smith, L., 1996, ApJ 463, 60
- Cayatte, V., Kotanyi, C., Balkowski, C., van Gorkom, J.H., 1994, AJ 107, 1003
- da Costa, L.N., Pellegrini, P.S., Davis, M., Meiksin, A., Sargent, W.L.W., Tonry, J.L., 1991, ApJS 75, 935
- de Vaucouleurs, G., de Vaucouleurs, A., Corwin, H.G., Buta, R.J., Paturel, G., Fouqué, P., 1991, Third Reference Catalogue of Bright Galaxies, Vols. I - III, Springer, New York (RC3)
- Drinkwater, M.J., Gregg, M., D., Colless, M., 2001a, ApJ 548, L139
- Drinkwater M.J., Gregg M.D., Holman, B., Brown, M., 2001b, MNRAS, in press
- Ferguson, H.C., 1989a, AJ 98, 367 (FCC)
- Ferguson, H.C., 1989b, Ap&SS 157, 227
- Ferguson, H.C., Binggeli, B., 1994, A&AR 6, 67
- Freedman, W.L., et al. 2001, ApJ 553, 47
- Fouqué, P., Bottinelli, L., Durand, N., Gouguenheim, L., Paturel, G., 1990, A&AS 86, 473
- Giovanelli, R., Haynes, M.P., 1985, ApJ 292, 404
- Guhathakurta, P., van Gorkom, J.H., Kotanyi, C.G., Balkowski, C., 1988, AJ 96 851
- Hamuy, M., Phillips, M.M., Maza, J., Wischnjewsky, M., Uomoto, A., Landolt, A.U., Khatwani, R., 1991, AJ 102, 208
- Haynes, M.P., Giovanelli, R., 1984, AJ 89, 758
- Heidmann, J., Heidmann, N., de Vaucouleurs, G., 1971, Mem. R. Astron. Soc. 75, 85
- Helou, G., Giovanardi, C., Salpeter, E.E., Krumm, N., 1981, ApJS 46, 267
- Helou, G., Hoffman, G.L., Salpeter, E. E., 1984, ApJS 55, 433
- Hoffman, G.L., Helou, G., Salpeter, E. E., Glosson, J., Sandage, A., 1987, ApJS 63, 247
- Hoffman, G.L., Helou, G., Salpeter, E. E., 1988, ApJ 324, 75
- Hoffman, G.L., Lewis, B.M., Helou, G., Salpeter, E. E., Williams, H.L., 1989, ApJS 69, 65
- Horellou, C., Casoli, F., Dupraz, C., 1995, A&A 303, 361
- Huchtmeier, W.K., Richter, O.-G., 1988, A&A 203, 237
- Huchtmeier, W.K., Richter, O.-G., 1989a, A&A 210, 1
- Huchtmeier, W.K., Richter, O.-G., 1989b, A General Catalog of HI Observations of Galaxies, Springer Verlag, New York (HR89)
- Jones, C., Stern, C., Forman, W., Breen, J., David, L., Tucker, W., Franx, M., 1997, ApJ 482, 143
- Killeen, N.E.B., Bicknell, G.V., 1988, ApJ 325, 165
- Kolatt, T., Dekel, A., Lahav, O., 1995, MNRAS 275, 797

- Lauberts, A., Valentijn, E.A., 1989, The Surface Photometry Catalog of the ESO-Uppsala galaxies, European Southern Observatory, Garching bei München
- Loveday, J., 1996, MNRAS 278, 1025
- MacGillivray, H.T., Beard, S.M., Dodd, R.J., 1988, *aldis. proc.* 389
- Marquarding, M., 2000, M.Sc. Thesis, Univ. of Melbourne
- Madore, B.F., et al., 1999, ApJ 515, 29
- Mathewson, D.S., Ford, V.L., Buchhorn, M., 1992, ApJS 81, 413
- McMahon, P., van Gorkom, J.H., Richter, O.-G., Ferguson, H.C., 1992, AJ 103, 399
- McMillan, R., Ciardullo, R., Jacoby, G.H., 1993, ApJ 416, 62
- Mould, J.R., et al., 2000, ApJ 528, 655
- Nilson, P., 1973, Uppsala General Catalog of Galaxies, Astr. Obs. Publ., Uppsala (UGC)
- Paturel, G., Fang, Y., Garnier, R., Petit, C., Rousseau, J., 2000, A&AS 146, 19
- Pierce, M.J., 1989, ApJ 344, L57
- Prosser, C.F., et al., 1999, ApJ 525, 80
- Putman, M., Bureau, M., Mould, J.R., Staveley-Smith, L., Freeman, K.C., 1998, AJ 115, 2345
- Richter, O.-G., Huchtmeier, W.K., 1984, A&A 132, 253
- Richter, O.-G., Sadler, E.M., 1985, A&AS 59, 433
- Sakai, S., Mould, J.R., et al., 2000, ApJ 529, 698
- Sandage, A., Tammann, G.A., 1981, 1987, A Revised Shapley-Ames Catalog of Bright Galaxies, Carnegie Institution Publ. 635, Washington (RSA)
- Schröder, A., 1995, Ph.D. Thesis, Univ. of Basel
- Schröder, A., Visvanathan, N., 1996, A&AS 118, 441
- Solanes, J.M., Giovanelli, R., Haynes, M.H., 1996, ApJ 461, 609 (SGH)
- Solanes, J.M., Manrique, A., García-Gómez, C., González-Casado, G., Giovanelli, R., Haynes, M.H., 2001, ApJ 548, 97
- Staveley-Smith, L., et al. 1996, PASA 13, 243
- van Gorkom, J.H., 1996, In: The Minnesota Lectures on Extragalactic Neutral Hydrogen, E.D. Skillman (ed)
- Visvanathan, N., 1983, ApJ 275, 430
- Waugh M., Webster R.L., Drinkwater, M.J., 2000, In: Mapping the Hidden Universe, R.C. Kraan-Korteweg, P.A. Henning, H. Andernach (eds), ASP Conf. Ser. 218, 231
- Wright, A.E., Otrupcek R., 1990, Parkes Catalogue, Monograph Australia Telescope National Facility (Publisher)

Appendix A: HI spectra

The HI spectra (uncalibrated) for all galaxies detected during our Parkes observations are shown in Fig. A.1. The calibration factor varied from year to year: 1.00 for 1991, 1.25 for 1992, 1.28 for 1993, and 1.32 for 1994. We show one spectrum per galaxy (because of the different set-ups per year we did not average the spectra of the different years), the others are available from one of the authors (Schröder).

During the 1993 and 1994 observing runs, data suffered frequently from strong interference at a central radial velocity of 1250 km s^{-1} . Negative spikes were excluded by range selection but positive spikes are sometimes easily visible in the plotted spectra.

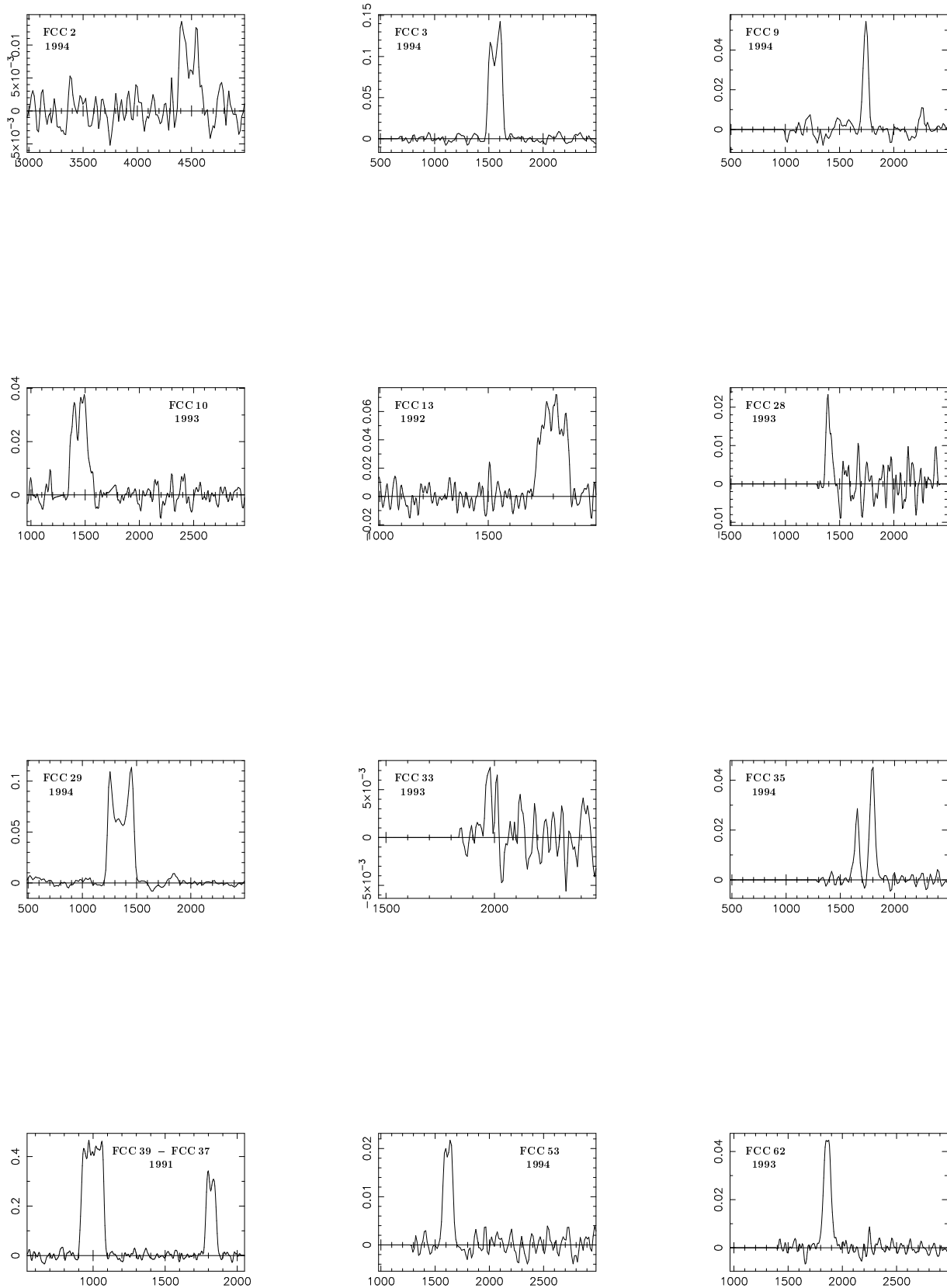


Fig. A.1. HI spectra of the detected galaxies in the Fornax cluster. In each plot the flux in mJy is plotted versus the velocity (optical convention) in km s^{-1} .

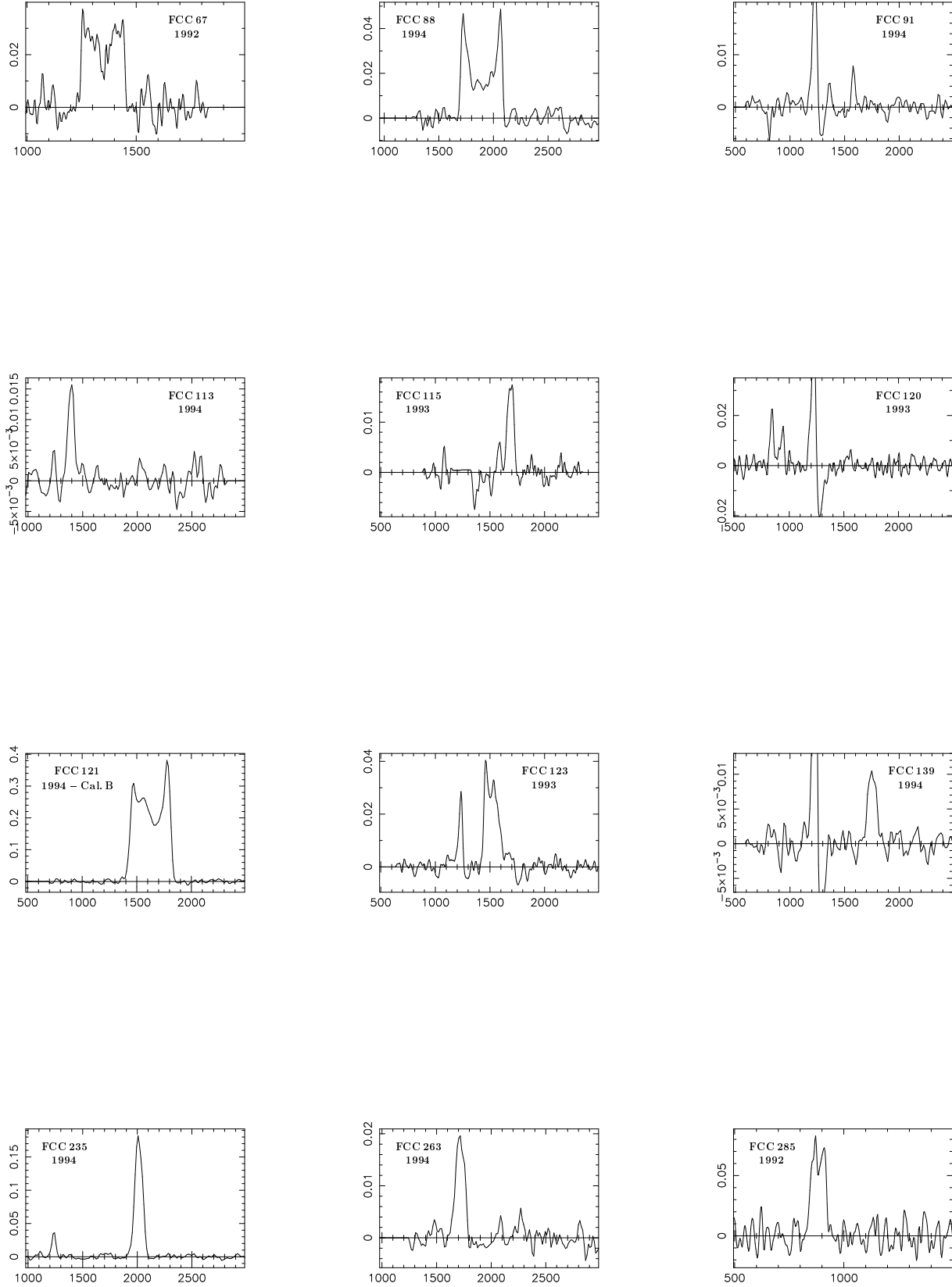


Fig. A.1. continued

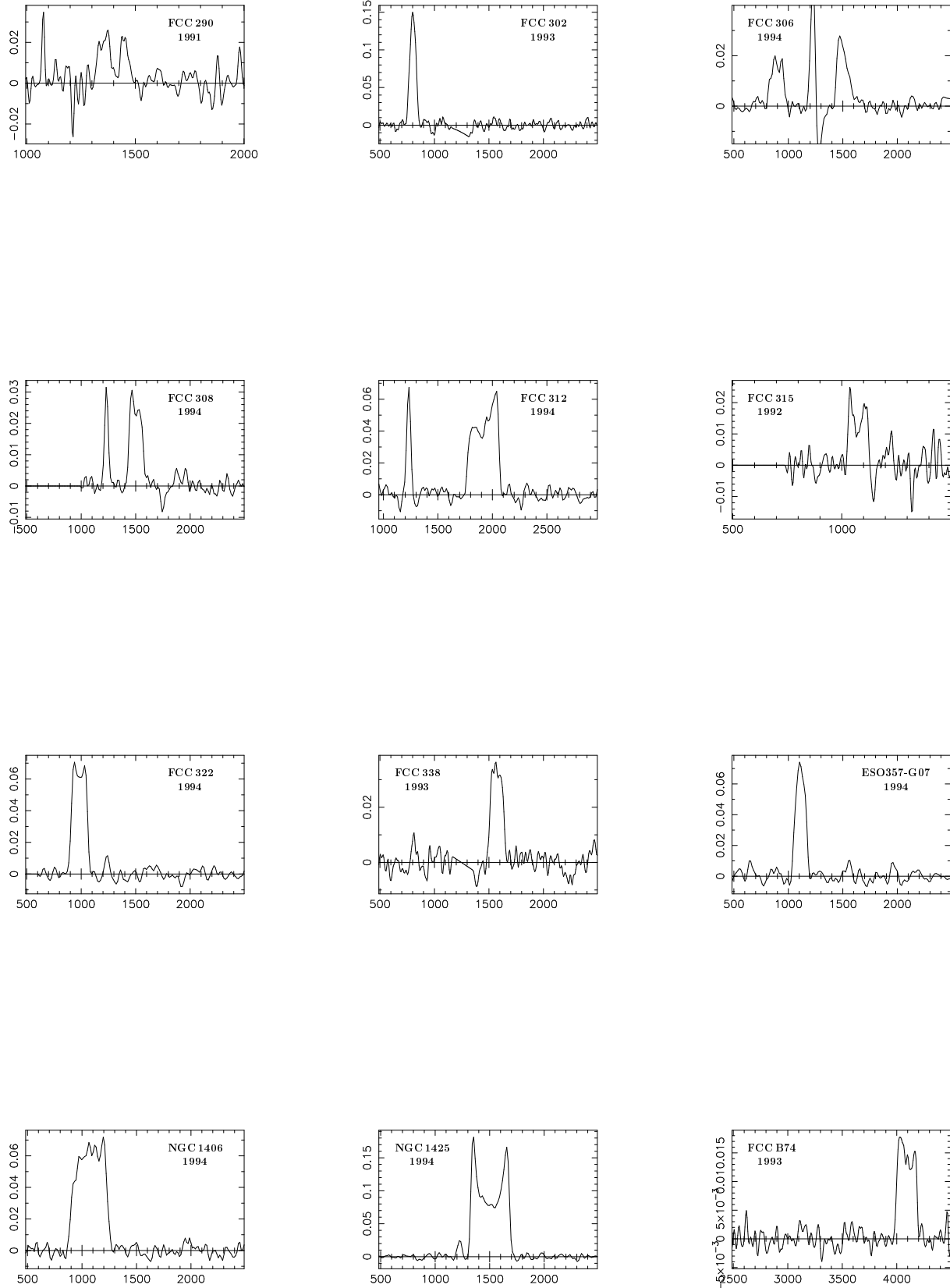


Fig. A.1. continued

Names:		Coordinates:			Velocity:				Linewidths:			Flux:				Remarks:			
FCC	Other	RA (J2000.0)	DEC	T	B_T	$\log D$	$\log R$	v_h	err	Δv_{50}	Δv_{25}	Δv_{20}	$\int S \cdot dv$	err	S_h	M_{HI}	S_{rms}	Run	Notes
					mag			kms/s		kms/s	kms/s	kms/s	Jy kms/s		Jy	$10^8 d_{20}^2 M_\odot$	m Jy		
(1a)	(1b)	(2a)	(2b)	(3)	(4)	(5)	(6)	(7a)	(7b)	(8a)	(8b)	(8c)	(9a)	(9b)	(10)	(11)	(12)	(13)	(14)
2	ESO 357-G10	3 15 42.5	-33 32 33	dSBc(LSB)	15.1	1.31	0.30	4540	9	178	189	191	2.43	1.02	0.023		4.69	91929394	
3	ESO 357-G12	3 16 53.8	-35 32 37	SBcd	14.1	1.66	0.24	1567	1	131	143	147	23.86	2.76	0.236	22.49	8.32	9294	
9		3 19 25.2	-32 39 15	Sd?	15.3	1.01	0.17 ^a	1751	3	52	65	68	4.91	1.01	0.096	4.63	8.78	919294	
10	IC 1913	3 19 34.4	-32 28 04	Sd	14.5	1.19	0.90	1450	3	159	179	181	6.76	1.00	0.057	6.37	4.74	919293	#
13	NGC 1310	3 21 01.0	-37 08 20	SBc	12.0	1.47	0.11	1808	3	125	135	137	9.38	1.77	0.099	8.84	13.51	919293	
21	NGC 1316	3 22 42.2	-37 12 36	S0 (pec)	9.4	1.85	0.18										16.72	93	Fornax A
22	NGC 1317	3 22 44.6	-37 06 17	Sa pec	11.9	1.66	0.13										10.17	94	
28	ESO 301-G11	3 23 54.4	-37 30 33	Sm	13.6	1.35	0.01	1405	5	45	57	61	1.44	0.60	0.047	1.36	11.54	919293	
29	NGC 1326	3 23 56.3	-36 27 58	SBa	11.8	1.49	0.18	1361	1	239	253	254	29.05	3.16	0.181	27.38	5.65	9294	
33	NGC 1316C	3 24 58.5	-37 00 34	Sd pec / BCD?	14.2	1.21	0.30	2000	5	60	63	63	0.59	0.49	0.013	0.56	3.60	91929394	
35		3 25 04.2	-36 55 39	Sm / BCD?	15.3	0.98	0.26 ^a	1800	1	35	55	56	2.63	0.60	0.065	2.48	3.58	91929394	
37	NGC 1326A?	3 25 09.1	-36 21 55	SBc (i.a.)	13.8	1.42	0.02	1831	1	70	82	84	23.84	2.55	0.364	22.47	7.23	919293	
39	NGC 1326B	3 25 19.9	-36 23 05	Sd (i.a.)	15.5	1.45	0.48	999	1	154	167	170	69.96	7.13	0.476	65.93	7.23	919293	
47	NGC 1336	3 26 32.1	-35 42 49	E4	13.3	1.53	0.17										9.99	91	
53	ESO 358-G05	3 27 16.3	-33 29 09	Scd	14.7	1.19	0.15	1628	4	94	108	111	3.08	0.78	0.037	2.90	5.12	9294	
62	NGC 1341	3 27 58.3	-37 08 57	Sbc	12.6	1.40	0.15	1876	3	60	87	90	4.48	0.66	0.064	4.22	3.57	919293	#
63	NGC 1339	3 28 06.7	-32 17 11	E4	12.7	1.47	0.15										14.76	91	
67	NGC 1351A	3 28 48.8	-35 10 49	Sc	13.0	1.35	0.70	1353	2	203	208	208	6.99	1.21	0.054	6.59	6.98	91929394	
76	ESO 358-G10	3 29 43.4	-33 33 26	Im / dS0	14.7	1.28	0.40										3.85	919293	
83	NGC 1351	3 30 35.2	-34 51 19	E5	12.3	1.46	0.19										7.80	9192	
88	NGC 1350	3 31 08.1	-33 37 47	SBb	11.8	1.77	0.27	1906	3	377	393	397	16.65	2.16	0.092	15.69	6.41	9294	
91		3 31 19.2	-32 03 13	Im	17.0	0.90	0.35 ^c	1590	12	22	40	44	0.41	0.36	0.015	0.39	3.50	9394	#
95		3 31 24.8	-35 19 51	dSB0 or dSBa	14.6	1.23	0.15 ^a										4.35	9294	
102		3 32 10.8	-36 13 14	Im	16.5	0.90	0.19 ^a										5.59	9294	*
113	ESO 358-G15	3 33 06.8	-34 48 32	Scd pec	15.2	1.09	0.25	1396	4	59	80	81	1.58	0.42	0.026	1.49	3.55	91929394	
115	ESO 358-G16	3 33 09.3	-35 43 05	Sdm	16.6	0.95	0.57	1700	4	65	84	87	1.74	0.53	0.031	1.64	3.17	91929394	
120		3 33 34.2	-36 36 20	Im	16.3	0.94	0.42 ^a	887	6	126	139	141	1.90	0.91	0.032	1.79	3.48	9394	
121	NGC 1365	3 33 36.3	-36 08 28	SBbc	10.2	1.93	0.15	1631	1	370	394	405	144.13	14.61	0.609	135.83	11.48	9294	
123		3 33 43.4	-35 51 32	Im	16.7	0.97	0.09	1540	4	135	172	179	6.27	0.96	0.058	5.91	3.76	9293	
128		3 34 07.1	-36 27 57	Im	16.8	0.87	0.20 ^a										6.42	94	*
139	ESO 358-G20	3 34 57.4	-32 38 22	SBm	14.4	1.27	0.18	1769	5	74	79	80	1.18	0.45	0.022	1.11	3.33	91929394	#
147	NGC 1374	3 35 16.9	-35 13 39	E0	11.9	1.21	0.03										12.84	91	
148	NGC 1375	3 35 16.9	-35 16 01	S0	13.6	1.37	0.36										12.84	9194	
152	ESO 358-G25	3 35 33.2	-32 27 50	S0/a pec	14.1	1.34	0.30										5.38	919293	*
153	IC 1963	3 35 31.1	-34 26 50	S0	13.0	1.40	0.62										13.58	91	
161	NGC 1379	3 36 04.1	-35 26 35	E0	11.7	1.35	0.02										13.35	91	
167	NGC 1380	3 36 27.6	-34 58 36	S0/a	11.3	1.42	0.22										4.99	929394	
176	NGC 1369	3 36 45.1	-36 15 22	SBa	13.7	1.35	0.05										4.52	91929394	*
177	NGC 1380A	3 36 47.5	-34 44 21	S0	13.2	1.39	0.57										6.00	919394	
179	NGC 1386	3 36 46.4	-36 00 02	Sa	12.4	1.48	0.42										4.57	91929394	
184	NGC 1387	3 36 57.0	-35 30 29	SB0	12.3	1.52	0.01										11.55	92	
193	NGC 1389	3 37 11.8	-35 44 45	SB0	12.8	1.49	0.29										3.84	9293	*
219	NGC 1404	3 38 52.2	-35 35 42	E2	10.9	1.45	0.11										14.70	91	
224		3 39 32.8	-31 47 30	Im or dE	16.9	0.91	0.16 ^b										3.90	94	
235	NGC 1427A	3 40 09.3	-35 37 28	Im	13.4	1.46	0.20	2028	1	78	106	113	23.25	2.52	0.295	21.91	6.18	9294	
240	ESO 419-G01	3 40 27.6	-31 41 07	Im	16.5	0.97	0.12										5.58	91929394	*
263	ESO 358-G51	3 41 32.3	-34 53 22	SBcd	14.6	1.23	0.40	1724	6	88	122	131	2.46	0.70	0.036	2.32	4.13	91929394	#
267		3 41 45.6	-33 47 29	Sm	16.0	1.06	0.14 ^a										4.79	929394	*
276	NGC 1427	3 42 19.3	-35 23 41	E4	11.8	1.24	0.14										7.58	91	
282		3 42 45.6	-33 55 12	Im / dE pec	14.5	1.17	0.08 ^a										4.44	94	*
285	NGC 1437A	3 43 02.0	-36 16 16	Sd	14.2	1.34	0.21	886	3	73	84	87	7.29	1.35	0.117	6.87	8.78	9294	
290	NGC 1437	3 43 37.1	-35 51 18	Sc	12.8	1.55	0.16	1406	11	131	159	161	2.15	0.91	0.025	2.03	5.96	91929394	
299		3 44 58.7	-36 53 40	Sd	17.1	0.84	0.55										3.99	929394	
302	ESO 358-G60	3 45 12.3	-35 34 14	Sdm	15.7	1.16	0.66	804	2	62	82	86	12.27	1.58	0.203	11.56	11.52	919293	
306		3 45 45.4	-36 20 45	SBm	15.6	0.79	0.18	886	5	90	115	116	2.66	0.67	0.036	2.51	3.25	91929394	
308	NGC 1437B	3 45 54.9	-36 21 30	Sd	13.8	1.42	0.48	1509	5	109	134	136	4.68	1.11	0.050	4.41	7.96	9294	
312	ESO 358-G63	3 46 19.0	-34 56 36	Scd	13.5	1.72	0.60	1929	2	286	295	297	20.93	2.64	0.109	19.72	8.78	9294	
315	IC 1993	3 47 04.7	-33 42 34	Sab	12.6	1.52	0.09	1080	3	91	99	100	2.03	0.51	0.035	1.91	4.53	91929394	
322	ESO 302-G09	3 47 33.2	-38 34 54	Sd	12.5	1.43	0.55	987	2	141	156	160	16.11	1.99	0.137	15.18	8.60	919294	
338	ESO 359-G03	3 52 01.1	-33 28 07	Sab	14.3	1.31	0.41	1582	6	127	146	152	5.64	1.20	0.049	5.32	4.98	93	
	NGC 1340	3 28 19.3	-31 04 04	E5	11.3	1.83	0.21										14.36	91	†
	ESO 357-G07	3 10 24.3	-33 09 22	SBm	14.6	1.42	0.85	1114	5	111	131	134	11.99	2.50	0.123	11.30	11.07	94	†
	NGC 1406	3 39 21.9	-31 20 24	SBbc	12.4	1.63	0.73	1074	5	325	355	363	30.47	3.98	0.112	28.71	7.77	94	†
	NGC 1425	3 42 11.4	-29 53 36	Sb	11.3	1.81	0.35	1513	1	355	370	374	56.49	5.89	0.291	53.24	6.04	94	†
B37		3 17 53.8	-33 03 40	BCD or S	14.9	0.85	0.11 ^c												

Notes: *: *FCC 102*: no v , small interf. at ~ 1200 and *FCC 121* at ~ 1650 ; *FCC 128*: no v , small interf. at ~ 1250 ; *FCC 152*: large interf. at ~ 1200 close to $v = 1465$ (Richter & Sadler 1985); *FCC 176*: large interf. at ~ 1250 close to $v = 1468$ (Richter & Sadler 1985); *FCC 193*: small interf. at ~ 800 and ~ 1200 , $v = 989$, should not be affected; *FCC 240*: no v , large interf. at ~ 1250 ; *FCC 267*: no v , large interf. at ~ 1250 ; *FCC 282*: small interf. at ~ 1250 close to $v = 1295$ (da Costa et al. 1991); *FCC B37*: no v , large interf. at ~ 1250 ; #: the second smallest line width has been adopted. †: $\log D$ is derived from RC3 values. Col. 5 ($\log R$): superscript a : axial ratio from Paturel et al. 2000, b : axial ratio from MacGillivray et al. 1988, c : axial ratio measured by the authors.